Semi-Calibrated Photometric Stereo

Donghyeon Cho, *Student Member, IEEE,* Yasuyuki Matsushita, *Member, IEEE,*
Yu-Wing Tai, *Member, IEEE,* and In So Kweon, *Member, IEEE*

Abstract—While conventional calibrated photometric stereo methods typically assume that light intensities are identical and sensor exposure is constant across observed images taken under varying lightings, these assumptions easily break down in practical settings due to individual light bulb's characteristics and limited control over sensors. In this paper, we study the effects of non-uniform light intensities and sensor exposures across observed images. In order to explicitly model these non-uniformities, we define "semi-calibrated" photometric stereo framework that light directions are assumed to be known or calibrated, but light intensities and exposures are variables to be estimated. Then, we propose methods for accurately determining surface normal in "semi-calibrated" photometric stereo framework. We consider how the new proposed concept, "semi-calibrated" photometric stereo, differs from conventional "uncalibrated" and "calibrated" photometric stereo and looks at its practical usefulness. In addition, we show that our methods are advantageous for general photometric stereo settings, where auto-exposure control is desirable. We compare our method with conventional Lambertian calibrated photometric stereo and robust photometric stereo methods as well as uncalibrated photometric stereo, and the experimental result shows superior accuracy of our method in this practical circumstance.

Index Terms—Photometric stereo, Light intensity, Exposure, Surface normal

1 Introduction

Non-uniform light intensities and exposures across observed images are a practical and common circumstance in data acquisition for photometric stereo that uses multiple images under distinct light directions. For example, different light bulbs with different intensity characteristics may be used for illuminating a scene. Even with identical light bulbs, due to that scene radiance is determined by surface normal and light directions, auto-adjusted sensor exposure is desirable depending on the light directions to avoid over-/under-exposures. Therefore, the capability of properly handling varying light intensities and exposures across observed images is an important feature for making photometric stereo more practical.

In the Lambertian image formation model, a measured intensity m is written as

$$m_{i,j} = E_i \rho_j \mathbf{n}_j^\top \mathbf{l}_i, \tag{1}$$

where i and j are indices of light direction and pixel location, $\mathbf{l}_i, \mathbf{n}_j \in \mathbb{R}^{3\times 1}$ are unit vectors of light direction and surface normal, $\rho_j \in \mathbb{R}$ is a Lambertian diffuse albedo, and $E_i \in \mathbb{R}$ is a light source intensity. In a matrix form for representing all pixels and light directions at a time, it can be written as

$$\mathbf{M} = \mathbf{E}\mathbf{L}\mathbf{N}^\top\mathbf{P}, \tag{2}$$

where $\mathbf{M} \in \mathbb{R}^{f\times p}$ is an observation matrix, $\mathbf{E}$ is an $f \times f$ diagonal light intensity matrix, $\mathbf{L} \in \mathbb{R}^{f\times 3}$ is a light direction matrix, $\mathbf{N} \in \mathbb{R}^{p\times 3}$ is a surface normal matrix, $\mathbf{P}$ is a $p \times p$ diagonal diffuse albedo matrix, and f and p are the number of images and pixels, respectively. Conventional photometric stereo [1] assumes that light source intensities are identical across images, where the matrix $\mathbf{E}$ becomes a scaled identity matrix ($\mathbf{E} = e\mathbf{I}$), and computes albedo-scaled surface normal $\mathbf{B}(= \mathbf{P}^\top\mathbf{N})$ by

$$e\mathbf{B}^{\top *} = \mathbf{L}^\dagger\mathbf{M}, \tag{3}$$

up to a scale ambiguity e, where the superscript † indicates a generalized inverse when $f \geq 3$.

Clearly, when the light source intensities are non-uniform or camera exposures vary across images, the assumption $\mathbf{E} = e\mathbf{I}$ does not hold, but instead its diagonal elements have individual scales. When this non-uniformity is present, the surface normal estimates by Eq. (2) naturally becomes biased by greater scales as illustrated in Fig. 1. While there are recently various robust estimation techniques used for photometric stereo [2], [3], [4], [5], [6], because the effect of non-uniform $\mathbf{E}$ neither increases the rank of the observation matrix nor sparsifies outliers, robust techniques such as rank minimization or ℓ_0-norm minimization techniques cannot resolve this issue. In the rest of the paper, we collectively call this problem setting, non-uniform light intensities and exposures across images, a *varying light intensity condition*, because they are both considered intensity scaling on individual images.

Under *varying light intensity condition*, as well as light direction, light intensity is the factor which is pre-calibrated or estimated with surface normal. Depending on whether the directions and intensities of light sources are calibrated, photometric stereo problem can be categorized into four cases: knowing both, not knowing both, and knowing only one of them. In this paper, we focus on a case that light directions are assumed to be known or calibrated, but light intensities and exposures are variables to be estimated. We call this case as "semi-calibrated" photometric stereo. We considers a method to effectively solve "semi-calibrated" photometric stereo under *varying light intensity condition*. The problem that we deal with in this paper is a bilinear problem written as following.

- *D. Cho and I.S. Kweon are KAIST, Daejeon, Korea. E-mail: cdh12242@gmail.com, iskweon@kaist.ac.kr*
- *Y. Matsushita is with Osaka University, Japan. E-mail: yasumat@ist.osaka-u.ac.jp*
- *Y-W. Tai is with Tencent Youtu, HongKong. E-mail: yuwing@gmail.com*

Manuscript received XXXX XX, XXXX; revised XXXX XX, XXXX.

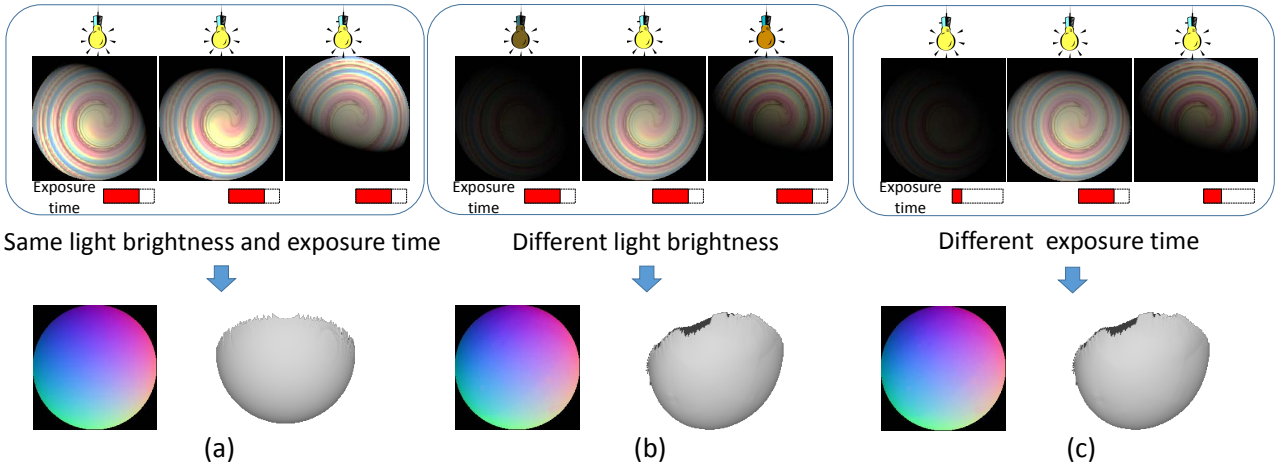

Fig. 1: (a) Conventional photometric stereo setting where constant light intensities and exposures are used, (b)(c): Varying lighting intensity/exposure conditions. Estimated surface normal are biased toward brighter light source or images captured with longer exposures with a conventional solution method.

Problem (Semi-calibrated photometric stereo under varying light intensity condition). *Given observations* $\mathbf{M}$ *and light directions* $\mathbf{L}$*, estimate a diagonal light intensity matrix* $\mathbf{E}$ *and an albedo-scaled surface normal matrix* $\mathbf{B}$ *from the following relationship:*

$$\mathbf{M} = \mathbf{ELB}^{\top}. \tag{4}$$

We first show that there exists a linear closed-form solution method, which simultaneously estimates scales of light intensities (or exposures) $\mathbf{E}$ and albedo-scaled surface normal $\mathbf{B}$. We call this method a linear joint estimation method. This method is straightforward to implement; however, inefficient in terms of computation time and memory consumption. We then introduce a factorization based method for determining only surface normal $\mathbf{B}$ in Eq. (4) without being affected by $\mathbf{E}$. It bypasses the estimation of $\mathbf{E}$ using algebraic distance minimization (or, cross product minimization) by making the problem independent of vector magnitudes. Next, we show that this bilinear problem can be efficiently solved by an alternating minimization technique that determines $\mathbf{E}$ and $\mathbf{B}$ in each step. Finally, in order to handle non-Lambertian components, we introduce robust alternating minimization method. We discuss details and characteristics of each method later in this paper.

We further show that our method is advantageous in improving signal-to-quantization-noise ratio (SQNR) in comparison to a standard photometric stereo method when an auto-exposure control is used, and as a result more accurate surface normal estimates can be obtained. Experimental results show the effectiveness of the proposed method in practical settings. In this paper, we assumes a directional light setting where radiance from a light source to a scene is constant except for shadowing, *i.e.*, spatially varying incident radiance within a scene is not assumed.

A shorter version of this work appeared in [7]. This paper extends our previous work with defining "semi-calibrated" photometric stereo, and additional experimentations. Also, the L1-norm based alternating minimization algorithm is newly introduced. To summarize, our contributions are as follows:

1) We introduce a concept of "semi-calibrated" photometric stereo under *varying light intensity condition*, and analyze differences with uncalibrated and calibrated photometric stereo.
2) In order to handle non-Lambertian components, we introduce robust alternating minimization method.
3) We evaluate our methods on new photometric stereo dataset, and demonstrate effectiveness of proposed methods.

2 Related Works

Photometric stereo was first introduced by Woodham [1] in 1980's for determining surface normal from images taken under known and varying light directions with a Lambertian reflectance assumption. After Woodham's work, there have been various techniques proposed for making photometric stereo more practical. Their main focuses are to relax the assumptions of (1) calibrated light sources and (2) Lambertian image formation model.

The first class of the methods, called uncalibrated photometric stereo, tries to eliminate the need for calibrating light directions. When the light directions are unknown, it is understood that the solution can be obtained up to a 3×3 linear ambiguity [8]. If the integrability [9] of the surface is assumed, it has been shown that the linear ambiguity can be reduced to a generalized bas-relief (GBR) ambiguity [10], which only has three parameters. To fully resolve these ambiguities, various types of external clues have been used. For example, there are methods that use the entropy of albedo distributions [11], specular observations [12], shadows [13], and groups of color and intensity profiles [14]. Our problem setting has a similarity to the uncalibrated photometric stereo scenario in that we relax the assumptions of known light intensities and *constant light intensity* across varying light directions. And none of the previous uncalibrated photometric stereo works can effectively solve the problem.

The second class of the methods tries to make photometric stereo applicable to non-Lambertian scenes. There are methods that use more sophisticated reflectance models than Lambertian reflectance model, such as the works that use Torrance-Sparrow [15], [16], Cook-Torrance [17], Phong [18], Blinn-Phong [19]. More recently, Shi *et al.* [20] propose a bi-polynomial reflectance model that produces successful results for non-Lambertian diffusive scenes. There are approaches that use robust estimation techniques by treating non-Lambertian reflectances and shadows as outliers. In [2], the robustness against outliers is achieved by capturing hundreds of input images coupled with Markov Random Field

(MRF) to maintain neighborhood smoothness. Verbiest and Van Gool [3] use a confidence approach to reject outliers in input images of photometric stereo. Wu *et al.* [4] proposed a robust method based on low-rank matrix factorization. Oh *et al.* [5] introduced a partial sum of singular values for rank minimization, and showed good performance in photometric stereo. Ikehata *et al.* [21] used a sparse Bayesian regression for effectively neglecting sparse outliers (specularities and shadows). While these techniques are effective, they are built upon the assumption of *constant light intensity*, and cannot directly address the issue of varying light intensities and exposures.

3 Categorization of Photometric Stereo

In this section, we categorize Lambertian photometric stereo into four cases depending on whether the directions and intensities of light sources are known. Also, we study effectiveness of each approach for non-uniform light intensities and exposures across images.

3.1 Calibrated Case

Usually, in conventional calibrated photometric stereo, light directions $\mathbf{L}$ are pre-calibrated while constant intensities across images are assumed. As a result, estimated surface normal can be globally biased toward brighter light source under non-uniform light intensities and exposures across images. In order to remove distortion from *varying light intensity condition*, light intensities $\mathbf{E}$ can be also pre-calibrated. However, sophisticated operations using Lambertian sphere are required to calibrate intensities of light sources. Taking into consideration that calibration using the chrome spheres to obtain directions of light sources, calibrating intensities of light sources using another Lambertian sphere in advance means that two different pre-calibration with two different types of spheres are required. It is very inefficient and makes photometric stereo impractical.

3.2 Uncalibrated Case

To make photometric stereo practical, in uncalibrated photometric stereo, surface normal, albedo, light direction and intensity are directly estimated from captured images without calibrating light directions and intensities in advance. Solutions of uncalibrated photometric stereo can be obtained via matrix factorization:

$$\mathbf{M} = \hat{\mathbf{S}}\hat{\mathbf{B}}^{\top}, \tag{5}$$

where $\hat{\mathbf{S}}$ and $\hat{\mathbf{B}}$ are *biased* intensity-scaled light direction and albedo-scaled surface normal, respectively. With an arbitrary 3×3 non-singular matrix $\mathbf{H}$, Eq. (5) can be re-written as

$$\mathbf{M} = (\hat{\mathbf{S}}\mathbf{H})(\mathbf{H}^{-1}\hat{\mathbf{B}}^{\top}). \tag{6}$$

Since any non-singular 3×3 matrix $\mathbf{H}$ satisfy Eq. (6), there is no unique solution for surface normal. Therefore, previous approaches [8], [9], [10], [11], [12], [13], [14] utilize prior knowledge about albedo or surface normal. In examples that satisfy prior assumptions, light direction and intensity are obtained as well as surface normal and albedo. However, when assumptions are violated, all of estimates become incorrect. In other words, uncalibrated photometric stereo lacks of generality even though it has benefits of practicality.

3.3 Hayakawa Case

As mentioned above, we touch cases that one of light directions and intensities is known. Firstly, we think of light intensity calibration without knowing light directions. As reported in [8] by Hayakawa *et al.*, if relative intensities across more than 6 frames are known, 3×3 non-singular matrix $\mathbf{H}$ can be computed by solving following relationship, $\left\|\hat{\mathbf{S}}\mathbf{H}\right\| = \hat{E}$ where $\hat{E}$ is known relative intensities. However, it depends on a few known intensities of some frames, and is vulnerable to errors and outliers. Also, as discussed later section Sec. 6, light intensity calibration is not easy as light direction calibration. To prevent confusion, we call this case as Hayakawa case.

3.4 Semi-calibrated Case with Known Light Direction

In this paper, we focus on a case that light directions are known or calibrated, but light intensities and exposures are variable to be estimated with albedo-scaled surface normal. We call it as "semi-calibrated" photometric stereo that can effectively handle non-uniform light intensities and sensor exposures across images. It is more practical than calibrated case and more general than uncalibrated photometric stereo. Also, unlike calibrated and Hayakawa cases, "semi-calibrated" photometric stereo is suitable to auto-adjusted sensor exposure function for avoiding over-/under-exposures because intensities of each frame are not fixed in advance. So far, since there is no studies that explictly focus on "semi-calibrated" photometric stereo under *varying light intensity condition*, we propose four solution methods in Sec. 4.

4 Semi-Calibrated Photometric stereo under varying light intensity conditions

As discussed in Eq. (4) and Sec. 3.4, we are interested in determining albedo-scaled surface normal $\mathbf{B}$ with unknown non-uniform scalings of light intensities or exposures $\mathbf{E}$. In a least-squares framework, the problem can be written as

$$\{\mathbf{E}^{*}, \mathbf{B}^{*}\} = \underset{\mathbf{E},\mathbf{B}}{\operatorname{argmin}} \|\mathbf{M} - \mathbf{E}\mathbf{L}\mathbf{B}^{\top}\|_{\mathrm{F}}^{2} \tag{7}$$

given the observations $\mathbf{M}$ and light directions $\mathbf{L}$.

We first present a linear estimation method that simultaneously estimates $\mathbf{B}$ and $\mathbf{E}$ in Sec. 4.1. We then describe a factorization based method in Sec. 4.2, which bypasses the estimation of unknown scalings $\mathbf{E}$. Then, we describe an efficient alternating minimization method in Sec. 4.3. Finally, we introduce robust alternating minimization method to handle non-Lambertian components.

4.1 Linear joint estimation method

The original form $\mathbf{M} = \mathbf{E}\mathbf{L}\mathbf{B}^{\top}$ can be re-written as $\mathbf{E^{-1}}\mathbf{M} = \mathbf{L}\mathbf{B}^{\top}$, because $\mathbf{E}$ is always invertible as it is a positive diagonal matrix. Given known $\mathbf{M}$ and $\mathbf{L}$, it can be viewed as a variant of a Sylvester equation [22]:

$$\mathbf{E}^{-1}\mathbf{M} - \mathbf{L}\mathbf{B}^{\top} = \mathbf{0}. \tag{8}$$

By vectorizing unknown variables $\mathbf{E}^{-1}$ and $\mathbf{B}^{\top}$, Eq. (8) can be written as

$$\begin{aligned}\left[\mathrm{diag}(\mathbf{m}_1)|\cdots|\mathrm{diag}(\mathbf{m}_p)\right]^{\top}\mathbf{E}^{-1}\mathbf{1} \\ - (\mathbf{I}_p \otimes \mathbf{L})\mathrm{vec}(\mathbf{B}^{\top}) = \mathbf{0},\end{aligned} \tag{9}$$

where $\mathrm{diag}(\cdot)$, $\mathrm{vec}(\cdot)$ and $\otimes$ are diagonalization, vectorization, and Kronecker product operators, respectively. $\mathbf{I}_p$ is a $p \times p$ identity matrix, and $\mathbf{1}$ indicates a vector whose elements are all one. By concatenating matrices and vectors in Eq. (9), a homogeneous equation can be obtained:

$$\underbrace{\left[-\mathbf{I}_p \otimes \mathbf{L} | \left[\mathrm{diag}(\mathbf{m}_1)| \cdots |\mathrm{diag}(\mathbf{m}_p)\right]^\top\right]}_{\mathbf{D}} \underbrace{\begin{bmatrix}\mathrm{vec}(\mathbf{B}^\top) \\ \mathbf{E}^{-1}\mathbf{1}\end{bmatrix}}_{\mathbf{y}} = \mathbf{0}, \quad (10)$$

where $\mathbf{D} \in \mathbb{R}^{pf \times (3p+f)}$ is a sparse design matrix and $\mathbf{y} \in \mathbb{R}^{(3p+f)\times 1}$ is an unknown vector. The homogeneous system always has a trivial solution $\mathbf{y} = \mathbf{0}$. To have a unique (up to scale) non-trivial solution, the matrix $\mathbf{D}$ should have a one dimensional null space, *i.e.*, when rank of $\mathbf{D}$ is $(3p + f - 1)$, a unique solution can be obtained via singular value decomposition (SVD). The minimum condition to have a unique solution up to scale is $f \geq 5$ and $p \geq 3$, or $f = 4$ and $p \geq 2$. Unlike conventional photometric stereo settings, increasing the number of light directions does not necessarily make the problem easier in this setting, because it also increases the unknowns about light intensities.

4.2 Factorization based method

Although the linear joint estimation method is simple to implement, it has practical limitations in terms of its computational time and memory requirement when the sparse matrix $\mathbf{D}$ is large; not only constructing $\mathbf{D}$ but also computing SVD of $\mathbf{D}$. This limitation can be relaxed by dividing the observation matrix into small groups and deriving solutions for each group. However, this grouping should be performed carefully to avoid the condition numbers of divided sub-matrices to be high. The condition number increases when observations within each divided group are similar to each other, and as a result, the numerical error becomes greater. To avoid these issues, we develop a factorization based method described in this section.

Like solution methods of uncalibrated photometric stereo, light directions and surface normal can be solved directly via matrix factorization as Eq. (5) and Eq. (6). In our setting, since we know the light directions $\mathbf{L}$, we can find an appropriate non-singular matrix $\mathbf{H}$ for resolving the biases. Regardless of the effect of light intensities, direction of $\hat{\mathbf{S}}\mathbf{H}$ should be the same with $\mathbf{L}$. Thus, we can use this constraint, $(\hat{\mathbf{S}}\mathbf{H}) \times \mathbf{L} = \mathbf{0}$ where $\times$ indicates a cross product for determining $\mathbf{H}$ as

$$\begin{bmatrix} 0 & -l_{i,3}\hat{\mathbf{s}}_i & l_{i,2}\hat{\mathbf{s}}_i \\ l_{i,3}\hat{\mathbf{s}}_i & 0 & -l_{i,1}\hat{\mathbf{s}}_i \end{bmatrix} \begin{bmatrix} \mathbf{h_1}^\top \\ \mathbf{h_2}^\top \\ \mathbf{h_3}^\top \end{bmatrix} = \mathbf{0}, \quad (11)$$

where $\mathbf{H} = [\mathbf{h_1}|\mathbf{h_2}|\mathbf{h_3}]$, $l_{i,*}$ and $\hat{\mathbf{s}}_i$ are i-th row of $\mathbf{L}$ and $\hat{\mathbf{S}}$, respectively. The solution of Eq. (11) is unique up to scale when there are more than 4 distinct light directions. Using estimated $\hat{\mathbf{H}}$, we can compute unbiased albedo-scaled surface normal $\mathbf{H}^{-1}\hat{\mathbf{B}}^\top$. Interestingly, this factorization based method can naturally bypass the light intensity estimation; thus, it is suitable for our setting. Compared to the linear joint estimation method, the computational cost of the factorization based method is lower, even without dividing observations $\mathbf{M}$ into small groups.

4.3 Alternating minimization method

While the previous two methods are effective in ideal settings, they are prone to large errors due to un-modelled observations, such as shadows and pixel saturations. To avoid this problem, we develop a robust method that is based on alternating minimization for solving Eq. (7).

Our method computes albedo-scaled surface normal $\mathbf{B}^{(t)}$ and non-uniform scalings $\mathbf{E}^{(t)}$ in an alternating manner using their intermediate estimates from the previous iteration. Using $\mathbf{E}^{(t)}$ from the previous iteration and by fixing it, albedo-scaled surface normal $\mathbf{B}^{(t+1)}$ is updated by

$$\mathbf{B}^{(t+1)} = \underset{\mathbf{B}}{\mathrm{argmin}} \left\| \mathbf{M} - \mathbf{E}^{(t)}\mathbf{L}\mathbf{B}^\top \right\|_{\mathrm{F}}^2. \quad (12)$$

The above problem is a linear problem with respect to $\mathbf{B}$ and can be solved efficiently. Once matrix $\mathbf{B}^{(t+1)}$ is determined, $\mathbf{E}^{(t+1)}$ is then updated by solving

$$\mathbf{E}^{(t+1)} = \underset{\mathbf{E}}{\mathrm{argmin}} \left\| \mathbf{M} - \mathbf{E}\mathbf{L}\mathbf{B}^{(t+1)^\top} \right\|_{\mathrm{F}}^2. \quad (13)$$

Since matrix $\mathbf{E}$ is diagonal, each element $E_i^{(t+1)}$ is simply determined by

$$E_i^{(t+1)} = \frac{\sum_j m_{i,j}(\mathbf{l}_i^\top \mathbf{b}_j{}^{(t+1)})^\top}{\sum_j (\mathbf{l}_i^\top \mathbf{b}_j{}^{(t+1)})(\mathbf{l}_i^\top \mathbf{b}_j{}^{(t+1)})^\top}. \quad (14)$$

The initial scaling matrix $\mathbf{E}^{(0)}$ is set to an identity matrix, and the convergence criteria is defined by the magnitude of variation of matrix $\mathbf{B}$, *i.e.*, $\|\mathbf{B}^{(t+1)} - \mathbf{B}^{(t)}\|_F < \epsilon$, where ϵ is set to a small value (in our implementation, $\epsilon = 1.0\text{e-}8$).

If we consider $\mathbf{E}$ as weights, this alternating minimization is similar to iteratively re-weighted least squares (IRLS) [23] except that weights are defined row-wise (each image has same weight). We show how the alternating method operates in the following. Let us consider updating $\mathbf{B}^{(t+1)}$ with fixing $\mathbf{E}^{(t)}$, then Eq. (12) becomes

$$\begin{aligned} \mathbf{B}^{(t+1)} &= \underset{\mathbf{B}}{\mathrm{argmin}} \left\| \mathbf{M} - \mathbf{E}^{(t)}\mathbf{L}\mathbf{B}^\top \right\|_{\mathrm{F}}^2 \\ &= \underset{\mathbf{B}}{\mathrm{argmin}} \left\| \mathbf{M} - \mathbf{E}^{*}\mathbf{L}\mathbf{B}^\top - \mathbf{E}^{r}\mathbf{L}\mathbf{B}^\top \right\|_{\mathrm{F}}^2, \end{aligned} \quad (15)$$

where $\mathbf{E}^{(t)} = \mathbf{E}^* + \mathbf{E}^r$, $\mathbf{E}^*$ is the ground truth (that we do not know), and $\mathbf{E}^r$ is the error from t-th iteration. It shows that the smaller the scaling error $\mathbf{E}^r$ is, the smaller objective cost becomes. The elements of $\mathbf{E}^{(t)}$ can also be written as

$$\begin{aligned} E_i^{(t)} &= \frac{\sum_j m_{i,j}(\mathbf{l}_i^\top \mathbf{b}_j{}^{(t)})^\top}{\sum_j (\mathbf{l}_i^\top \mathbf{b}_j{}^{(t)})(\mathbf{l}_i^\top \mathbf{b}_j{}^{(t)})^\top} \\ &= \frac{\sum_j m_{i,j}\mathbf{l}_i^\top \mathbf{b}_j{}^{*\top} + \sum_j m_{i,j}\mathbf{l}_i^\top \mathbf{b}_j{}^{r\top}}{\sum_j (\mathbf{l}_i^\top (\mathbf{b}_j{}^* + \mathbf{b}_j{}^r)^\top)(\mathbf{l}_i^\top (\mathbf{b}_j{}^* + \mathbf{b}_j{}^r)^\top)}, \end{aligned} \quad (16)$$

where $\mathbf{b}^{(t+1)} = \mathbf{b}^* + \mathbf{b}^r$, $\mathbf{b}^*$ is the ground truth, and $\mathbf{b}^r$ is the error from t-th iteration. Since the denominator is fixed for all images, and the left-hand side of the numerator is proportional to the ground truth scaling $\mathbf{E}^*$, the smaller the error $\mathbf{b}^r$ becomes, the better scaling elements E becomes. To summarize, if the current estimate of albedo-scaled surface normal $\mathbf{B}^{(t)}$ is better than the previous one, $\mathbf{E}^{(t)}$ is better updated. In our experiments, above improvements are always observed since updated $\mathbf{E}^{(1)}$ becomes closer to the ground truth than $\mathbf{E}^{(0)}$. Then, $\mathbf{B}^{(t)}$ and $\mathbf{E}^{(t)}$ are alternatingly updated. The minimum condition for obtaining a stable solution is experimentally found to be $f \geq 5$ and $p \geq 3$.

4.4 Robust Alternating minimization method

solving Eq. (7) by the linear joint estimation, factorization based, alternating minimization (AM) can be biased by outliers. One possible solution to resolve outliers, is to reformulate Eq. (7) as

$$\{\mathbf{E}^*, \mathbf{B}^*\} = \underset{\mathbf{E},\mathbf{B}}{\operatorname{argmin}} \|\mathbf{M} - \mathbf{E}\mathbf{L}\mathbf{B}^\top\|_1. \tag{17}$$

In order to solve L1-norm minimization in Eq. (17), we adopt iteratively re-weighted least squares (IRLS) [23]. At each iteration, we multiply a weight value for each pixel. Pixels that are considered outliers are multiplied by small weights, and pixels considered inliers are multiplied by high weights. Therefore, Eq. (12), and Eq. (13) are modified as

$$\mathbf{B}^{(t+1)} = \underset{\mathbf{B}}{\operatorname{argmin}} \left\| \mathbf{W}^{(t)} \odot (\mathbf{M} - \mathbf{E}^{(t)}\mathbf{L}\mathbf{B}^\top) \right\|_{\mathrm{F}}^2, \tag{18}$$

$$\mathbf{E}^{(t+1)} = \underset{\mathbf{E}}{\operatorname{argmin}} \left\| \mathbf{W}^{(t)} \odot (\mathbf{M} - \mathbf{E}\mathbf{L}\mathbf{B}^{(t+1)^\top}) \right\|_{\mathrm{F}}^2, \tag{19}$$

where $\mathbf{W}^{(t)}$ is weight matrix and $\odot$ element-wise multiplication.

Weight matrix is defined as

$$\mathbf{W}^{(t)} = \gamma \cdot \max(|(\mathbf{M} - \mathbf{E}^{(t-1)}\mathbf{L}\mathbf{B}^{(t-1)^\top})|, \beta)^{-1}, \tag{20}$$

where γ, and β are a scaling factor and a thresholding value, respectively. Compared to proposed three methods in Sec. 4.1, Sec. 4.2 and Sec. 4.3, L1-based robust method can take care about sparse outliers effectively.

5 Signal-to-Quantization-Noise ratio analysis

One of the important benefits of our method is its compatibility to the sensor's auto-exposure function that makes non-uniform scaling of observations. With auto-exposure, SQNR of observations is effectively increased by avoiding over-/under-exposures. As a result, the surface normal estimates are less suffered from quantization noise, and thus, a greater accuracy can be obtained. Based on the previous study of quantization noise [24], SQNR is written as

$$SQNR = \frac{signal}{noise} \propto \frac{C\mu}{\frac{CR}{Q}} = \frac{Q\mu}{R} = \frac{Q\mu}{(V_h - V_l)}, \tag{21}$$

where μ is the expectation of the signal, Q is the number of quantization levels, and C is a scaling factor representing the amount of exposure. Also, $R = V_h - V_l$, where V_l and V_h are the minimum and maximum scene irradiance. Thus, R and μ are both the functions of exposure time. From Eq. (21), we can observe that SQNR without saturation is dependent of the number of quantization levels Q; thus, better exposed signals produce a higher SQNR.

When the signals are over-exposed, the SQNR expression becomes more complicated due to saturation, as

$$SQNR = \frac{signal}{noise} \propto \frac{C_o\mu - \alpha}{\frac{(\lambda - C_oV_l)}{Q} + \alpha}, \tag{22}$$

where λ, α, and C_o are saturation threshold, expectation of error within saturation sub-interval, and scaling factor of the over-exposure case, respectively. Here, C_oV_h is replaced by λ due to the saturation.

Let us assume that not all signals are saturated. Then, the condition that the well-exposed case has a greater SQNR than the over-exposed case is following:

$$\frac{Q\mu}{(V_h - V_l)} \geq \frac{C_o\mu - \alpha}{\frac{(\lambda - C_oV_l)}{Q} + \alpha} = \frac{C_oQ\mu - Q\alpha}{\lambda - C_oV_l + Q\alpha}. \tag{23}$$

Above can be simplified by some algebraic operations into:

$$\frac{Q\mu}{(V_h - V_l)} \geq \frac{Q\alpha}{(C_oV_h - \lambda) - Q\alpha}. \tag{24}$$

The condition to satisfy Eq. (23) with respect to Q is

$$Q \leq \frac{(C_oV_h - \lambda)}{\alpha} - \frac{(V_h - V_l)}{\mu}, Q > \frac{(C_oV_h - \lambda)}{\alpha}, \tag{25}$$

where $(C_oV_h - \lambda)$ is the maximum error. Mathematically, over-exposed case can produce higher SQNR than well-exposed case. However, in general situations, SQNR of well-exposed case is better than over-exposed case because the number of quantization levels Q is usually larger enough than maximum error $(C_oV_h - \lambda)$ over expectation error α. Therefore, well-exposed signals have higher SQNR than over- or under-exposure cases in terms of quantization if the number of quantization levels is sufficient. Then, our methods are beneficial with auto-exposure to increase SQNR since it can handle non-uniformity caused by auto-exposure effectively.

If there are quantization noise in the images, the observation matrix $\mathbf{M}$ becomes

$$\mathbf{M} = \mathbf{M}^* + \zeta = \mathbf{E}\mathbf{L}\mathbf{B}^\top + \zeta, \tag{26}$$

where $\mathbf{M}^*$ and ζ are the ideal observation and quantization noise, respectively. Using the noisy input in Eq. (26) , the objective function in Eq. (7) becomes

$$\{\mathbf{E}^*, \mathbf{B}^*\} = \underset{\mathbf{E},\mathbf{B}}{\operatorname{argmin}} \|\zeta\|_{\mathrm{F}}^2, \quad \text{s.t.} \quad \zeta = \mathbf{M} - \mathbf{E}\mathbf{L}\mathbf{B}^\top. \tag{27}$$

Therefore, in the cases of high SQNR data, we can compute surface normal and intensities by optimizing Eq. (27) without biases since ζ is close to zero ($\mathbf{M} \approx \mathbf{M}^*$). However, in low SQNR inputs, minimizing Eq. (27) can produce biased results because ζ is not small anymore ($\mathbf{M} \neq \mathbf{M}^*$). As a result, auto-exposure can help to estimate surface normal by increasing SQNR of images, and our method is suitable for dealing with the exposure variations.

6 Light intensity calibration analysis

One may think that light intensity calibration is an easy task, but it actually requires both careful control over the environment and explicit knowledge about the reflectance of a calibration target. To show this, we perform light intensity calibration using a diffuse sphere[1]. Assuming a Lambertian reflectance model and known surface normal $\mathbf{N}$, the scaled light matrix $\mathbf{S}$ can be estimated from a set of measurements $\mathbf{M}$ as

$$\mathbf{S}^* = \underset{\mathbf{S}}{\operatorname{argmin}} \left\| \pi_{\Omega^c}(\mathbf{M}) - \pi_{\Omega^c}(\mathbf{S}\mathbf{N}^\top) \right\|_{\mathrm{F}}^2, \tag{28}$$

where Ω denotes the locations of shadowed entries in the observation $\mathbf{M}$, and π_{Ω^c} represents an operator that extracts entries

1. Due to the presence of saturations, a chrome sphere with specular highlights is not a proper calibration object for this task.

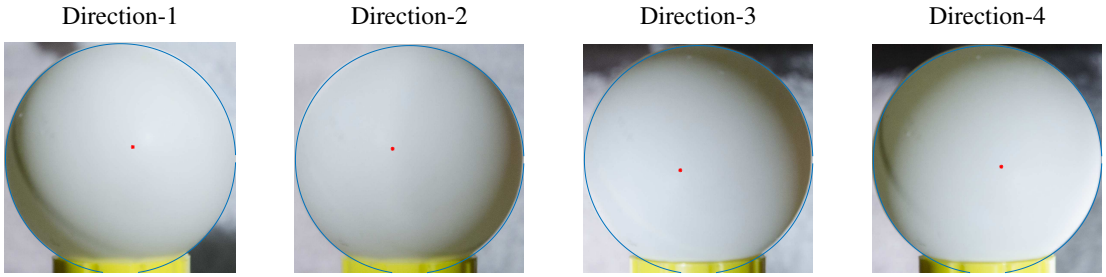

(a) 1.0 (b) 0.948 (c) 0.939 (d) 0.988

Fig. 2: Light intensity calibration. A diffuse sphere is illuminated under different light directions by moving an identical light source. The red point indicates the lighting direction, and a blue circle is a circle fitting to the image of a sphere. The numbers under photographs are the estimated light source intensities, that are relative to that of Direction 1.

that are not shadowed (Ω^c). Since $\mathbf{S} = \mathbf{EL}$, with known light directions $\mathbf{L}$, we can determine the light intensities by

$$\mathbf{E} = \mathbf{S}^* \mathbf{L}^\dagger. \tag{29}$$

We recorded images of a diffuse sphere by changing the light directions of an identical light source with retaining its distance to the target object approximately the same. The camera response function is linear and uncompressed RAW images are used. Exposure times are set constant with making sure that there is no under- or over-exposures. In addition, to neglect the perspective effect, a camera is placed far enough from the target object so that we can assume an orthographic projection model. Fig 2 shows some of the recorded images, and the light intensity matrix $\mathbf{E}$ is obtained by Eqs. (28) and (29).

As summarized in the numbers in Fig. 2, the estimated light intensities have variations while they are supposed to be uniform under this setting. The variations may be caused due to that (1) although the sphere is carefully selected, it still deviates from the Lambertian assumption, and (2) the assumed surface normal directions may be different from the truth due to errors of circle fitting. As such, even with a careful procedure, the light source intensity calibration is not a straightforward task. And in our setting, it had a non-negligible spread of estimated intensities (maximum 0.052 when the intensities are normalized to one, corresponding to 5% error). Therefore, it is needed to directly model the variations of light intensities in the photometric stereo formulation.

7 Experiments

We evaluate the proposed methods, linear joint estimation, factorization based, alternating minimization (AM), and robust alternating minimization (Robust-AM) methods, using synthetic (Sec. 7.1), benchmark (Sec. 7.2), and real-world (Sec. 7.3) scenes in the setting of non-uniform intensities and exposures. Although none of the previous techniques are designed for the non-uniform intensity setting, as previous methods to compare, we use standard Frobenius-norm minimization [1], robust L1-norm minimization used as a baseline method in [25], and the state-of-the-art photometric stereo algorithm based on constrained bivariate regression (CBR) [25].

7.1 Synthetic data

We first test our methods using synthetic examples that are textured and rendered with a Lambertian reflectance model with shadows. For qualitative and quantitative comparisons, we analyze the effects of non-uniform light intensities and auto-exposure. In addition, we demonstrate how well previous and proposed methods handle non-Lambertian components.

Non-uniform light intensities: We first test the setting of non-uniform light intensities. The scenes are rendered under 20 varying light directions with their intensity variance 0.05. The qualitative visualization of surface normal estimates and error maps are summarized in Fig. 3 with comparison to other previous methods, *i.e.*, Frobenius-norm, L1-norm, CBR. Our methods, namely, linear joint, Factorization, and AM methods correspond to the ones described in Secs. 4.1, 4.2, and 4.3, respectively. Our proposed methods produce results close to the ground truth compared to other techniques that do not explicitly consider the non-uniform light intensities. The quantitative results are reported under each error map. The superior performance is consistently observed under varying numbers of images and light intensity variances as shown in Fig. 4.

Auto-exposure case: Auto-exposure allows us to obtain measurements with a higher Signal-to-Quantization-Noise ratio (SQNR). To assess the benefit of auto-exposure in photometric stereo and effectiveness of our methods in this setting, we render two datasets; one with auto-exposure and the other with fixed-exposure. In the auto-exposure dataset, the sensor irradiances are stretched to properly include the most of dynamic range before quantization. For the fixed-exposure dataset, sensor irradiances are quantized without stretching. From the two types of dataset, we apply the same set of photometric stereo methods for performance evaluation. The results are summarized in Table. 1. While the fixed-exposure setting suffers from a low SQNR (which leads to lower accuracy of surface normal estimates), the auto-exposure retains a higher SQNR. And with our methods, this setting is properly handled and accurate surface normal estimates are obtained.

Non-Lambertian cases: Since our proposed methods, especially, linear joint estimation and factorization based method are general solutions for ideal Lambertian objects, it is difficult to deal with non-Lambertian components. In order to see how well our four methods cope with non-Lambertian components, we perform experiments on non-Lambertian examples under non-uniform light intensities. To render non-Lambertian examples, we adopt Cook-Torrance model [17]. Similar to Lambertian cases, we produce 20 images which are rendered varying light directions and intensities as shown Fig. 5. Input images have a lot of non-Lambertian regions and saturated pixels. Fig. 5 shows qualitative and quan-

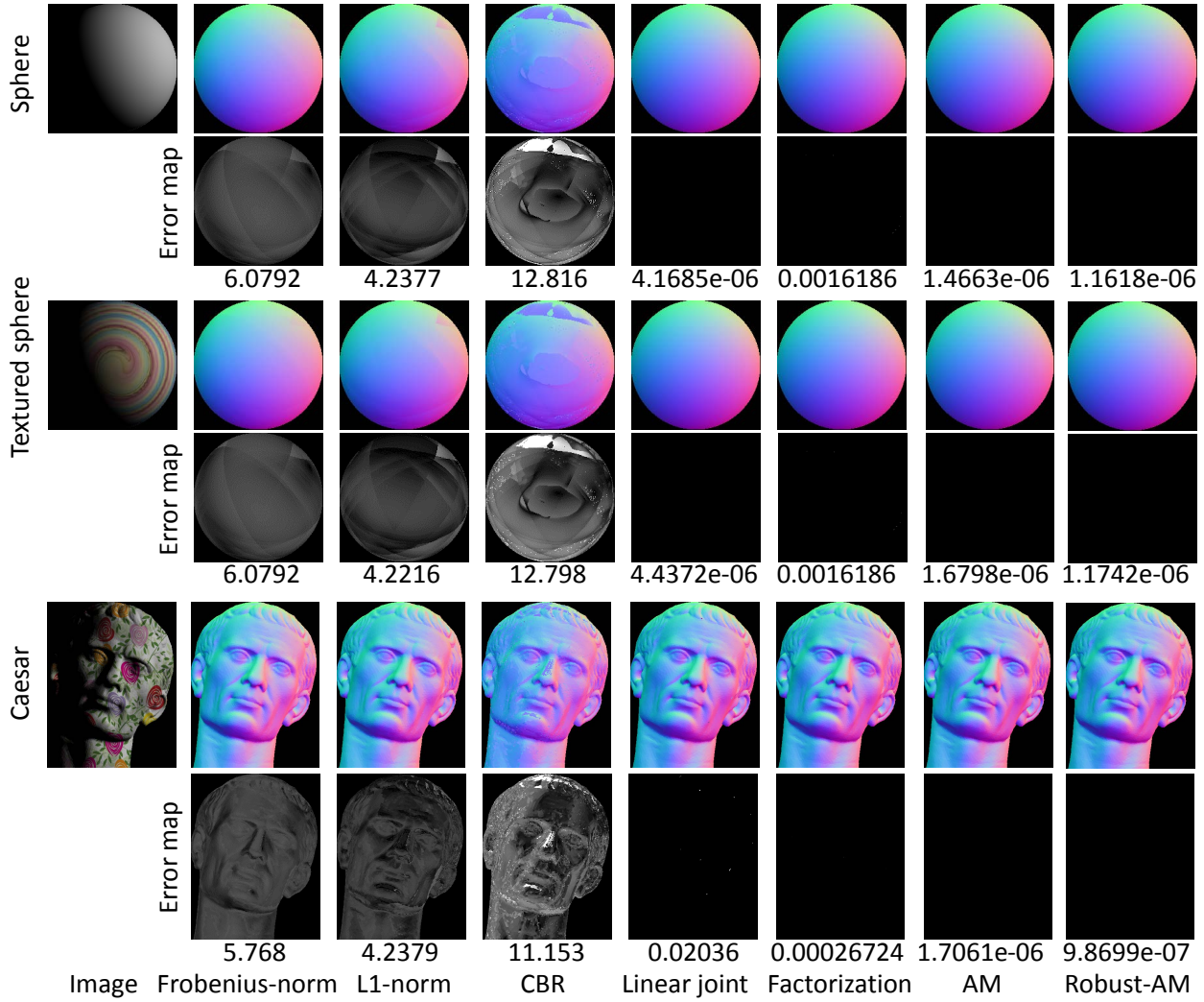

Fig. 3: (Lambertian cases) Photometric stereo experiment under non-uniform light intensities. The scenes are rendered under 20 distinct light directions with their intensity variance 0.05. Our methods (linear joint, factorization, AM and Robust-AM) effectively handle the condition of non-uniform light intensities. Error maps are scaled by 4 times. The numbers indicate the mean angular errors in degree.

titative comparisons with other previous methods. Linear joint and factorization based methods are severely broken down while previous method cannot deal with non-uniform light intensities. Compared to other methods, AM and Robust-AM methods effectively handle non-uniform light intensities and non-Lambertian components.

7.2 Benchmark data

Shi *et al.* [26] provide photometric stereo dataset which contains 10 sets of input images, calibrated light directions, intensities for each image as well as ground truth surface normals. Unlike dataset in Sec. 7.1, input images are not synthetic, and also contain noise and outliers. Dataset covers various types of surface such as complicated BRDF and spatially-varying materials. Since their images are captured under *varying light intensity condition*, it is appropriate to experiment our proposed methods on their dataset. Table. 2 shows angular errors of each method for each example. In the most of examples, AM and robust-AM methods produce smaller errors than previous methods which do not consider non-uniform light intensities and sensor exposures. However linear joint method is vulnerable to outliers and easily broken down. Interestingly, for complicated cases (POT2, COW, HARVEST), our methods are not much different from conventional methods or rather are not good. Surface materials of those examples are spatially-varying or complicated, thus consideration for non-Lambertian and outliers is more critical factor than non-uniform intensities and sensor exposures. Because our methods are solutions to the basic Lambertian model, considering non-uniform intensity to an example such as the Harvest, which includes a considerable number of outliers, can have a negative impact on the results. In most cases, however, handling non-uniform intensities can be made for non-Lambertian objects with an simple method such as L1-norm minimization Sec. 4.4.

7.3 Real data

We design three different settings for the real-world experiment; (A) non-uniform light source intensities across images, (B) recording with auto-exposures under identical light intensities (by moving the same light source), and (C) use of an uncontrolled mobile phone camera for imaging where auto-exposure is turned on under varying light source intensities. For all real-world examples, we use a shiny sphere to calibrate the light directions. To suppress

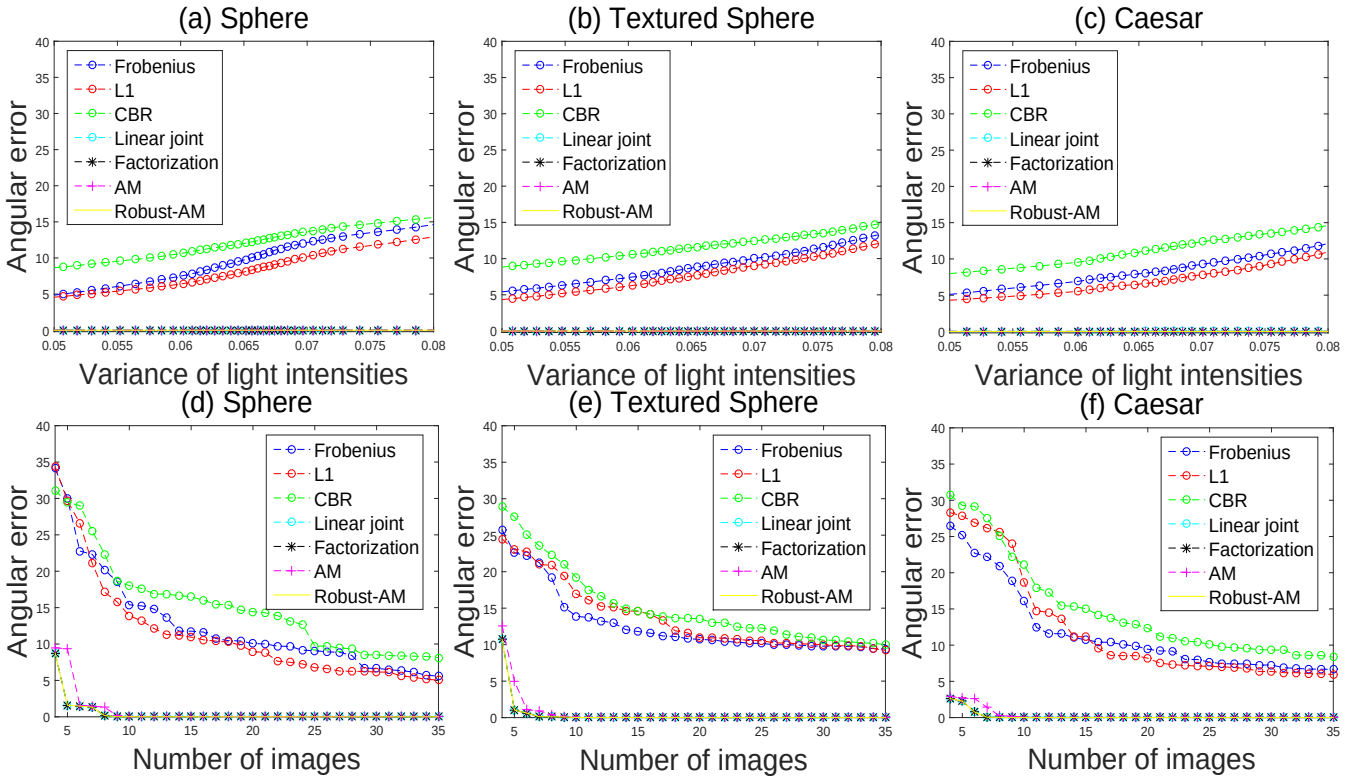

Fig. 4: Variations of mean angular errors of surface normal estimates over variance of light intensities (top row) and the number of images (bottom row) for the three datasets. (a,d) Sphere, (b,e) Textured Sphere, (c,f) Caesar. Our methods consistently yield favorable results across these variations.

	Sphere		**Textured**		**Caesar**	
	Fixed	**Auto**	**Fixed**	**Auto**	**Fixed**	**Auto**
SQNR	48.395	126.47	42.992	126.65	41.676	128.7
Frobenius	1.347	24.865	1.9296	24.989	2.6284	24.434
L1	1.5052	24.355	2.135	24.481	2.8427	21.853
CBR [25]	17.292	14.464	19.599	14.752	20.878	21.514
Linear joint	9.2883	0.80469	13.351	0.80413	11.667	2.4814
Factorization	2.699	0.71346	4.3541	0.73457	5.8064	2.36
AM	2.1928	**0.15501**	3.0471	**0.16254**	3.4081	**0.41689**
Robust-AM	2.2852	**0.15501**	3.1601	**0.16254**	3.5626	**0.41689**

TABLE 1: Comparison under auto-exposure (Auto) and fixed-exposure (Fixed) settings. SQNR and the mean angular errors of surface normal estimates in degree are shown.

other disturbing factors, our experiments are carried out in a dark room.

Non-uniform light source intensities: To record images under different light intensities and directions, we use controllable light sources whose brightnesses can be manually controlled by the gain of power supply. The camera setting, such as shutter speed and aperture, are all fixed in this experiment, and a linear sensor response is used. In this experimental setting, we record 20 images for each static scene. The results are summarized in Fig. 6, in which the estimated surface normal and their 3D reconstruction using [27] are presented. As shown in the figures, our methods properly handle the varying light source intensities compared to Frobenius-norm, L1-norm and CBR methods, with which severe distortions are observed in their reconstructed surfaces.

Auto-exposure: When auto-exposure is used, the shutter speed and/or aperture size of a camera is automatically adjusted to record well-exposed images according to the amount of incoming light. While it increases SQNR, it results in the non-uniform intensity setting.

For this experiment, we record 20 images of each static scene with auto-exposure. Fig 7 shows the comparative result. As shown in the figure, our methods consistently yield higher quality outputs than the other methods because our method explicitly accounts for the non-uniform exposures.

Mobile phone cameras: Our method is suitable for uncontrollable cameras like many of mobile phone cameras, where we cannot turn off the auto-exposure setting. With such cameras, recorded images are in the condition of non-uniform exposures across images. From recorded images from a mobile phone camera, we linearize the intensity observations using the method of [28] as preprocessing. Fig 8 shows the surface normal estimates and their 3D reconstructions. While the 3D reconstructions of conventional methods are severely deformed, our methods show better

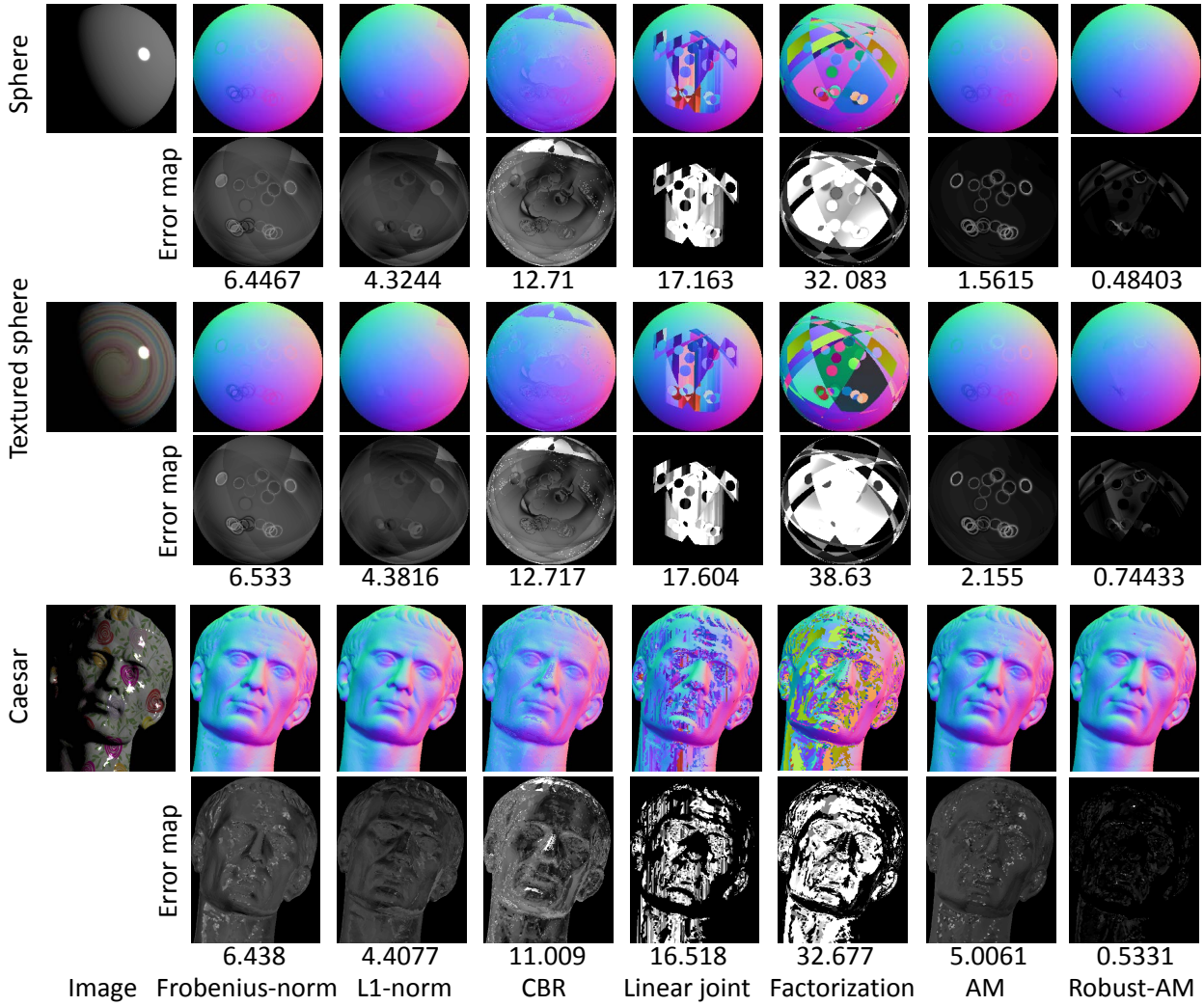

Fig. 5: (Non-Lambertian cases) Photometric stereo experiment under non-uniform light intensities. The scenes are rendered under 20 distinct light directions with their intensity variance 0.05. Our methods (linear joint, factorization, AM and Robust-AM) effectively handle the condition of non-uniform light intensities. Error maps are scaled by 4 times. The numbers indicate the mean angular errors in degree.

reconstructions in general. The linear joint estimation method suffered from the outliers in this case, but that is not observed in factorization based and AM methods.

7.4 Difference from spatially-varying light case

Spatially-varying light intensities can be caused by near-light or non-isotropic light source cases, and there are a few approaches to dealing with this [29], [30], [31]. As stated, our setting is different from the near-light setting, and we primarily consider the situation where the directional light intensities are different *across* images. The setting is not a subset of the spatially-varying light case, and to verify the difference, we show the results of applying our method and the NLPS method [29] to both spatially-varying (near-light) and non-uniform light (our setting) cases. The results are summarized in Table. 3. This result is rather natural in that the near-light setting is better handled by NLPS [29], while the non-uniform light case (our setting) cannot be dealt well with the method based on the near-light assumption, because these are two distinct settings.

8 Conclusion

This paper described photometric stereo methods that can handle the non-uniform light source intensities and exposures across images. We showed the effect of *varying light intensity conditions* in photometric stereo that is relevant in practical settings. We then developed solution methods that explicitly account for the non-uniform light intensities and exposures; namely, linear joint estimation, factorization based, alternating minimization, robust alternating minimization methods. The linear joint estimation and factorization based methods are simple and easy to implement, they occasionally suffer from numerical instability due to un-modelled observations. The alternating minimization method showed a greater robustness over these techniques, while retaining the efficiency in computation. The robust-AM methods effectively handle sparse outliers which cannot be detected by linear joint estimation, factorization based, and AM methods. They are all effective in the non-uniform intensities setting compared to methods that neglect the effect of the setting. We further illustrate that our proposed methods can benefit from auto-exposure, with which measurements with a greater SQNR can be obtained. Our experiments on synthetic and real-world examples show the importance

	Frobenius	L1	CBR [25]	Linear joint	Factorization	AM	Robust-AM
BALL	16.7	19.107	18.618	30.057	4.6221	3.746	**2.7766**
CAT	17.34	19.427	18.856	18.566	8.9488	8.8481	**8.0482**
POT1	18.344	19.308	18.968	14.752	9.6366	9.622	**9.4654**
BEAR	20.863	22.045	23.01	26.026	9.5641	9.2638	**8.0717**
POT2	21.562	21.481	20.837	38.158	20.169	19.652	**19.584**
BUDDA	20.946	22.852	21.485	34.408	15.229	15.113	**13.378**
GOBLET	23.298	23.643	23.299	47.509	23.428	22.563	**18.184**
READING	24.877	24.434	24.906	55.759	20.207	18.639	**14.185**
COW	26.976	27.347	25.942	47.61	28.5	28.307	**26.896**
HARVEST	**33.089**	33.424	31.831	48.697	45.017	41.224	33.347

TABLE 2: Comparison under auto-exposure (Auto) and fixed-exposure (Fixed) settings. SQNR and the mean angular errors of surface normal estimates in degree are shown.

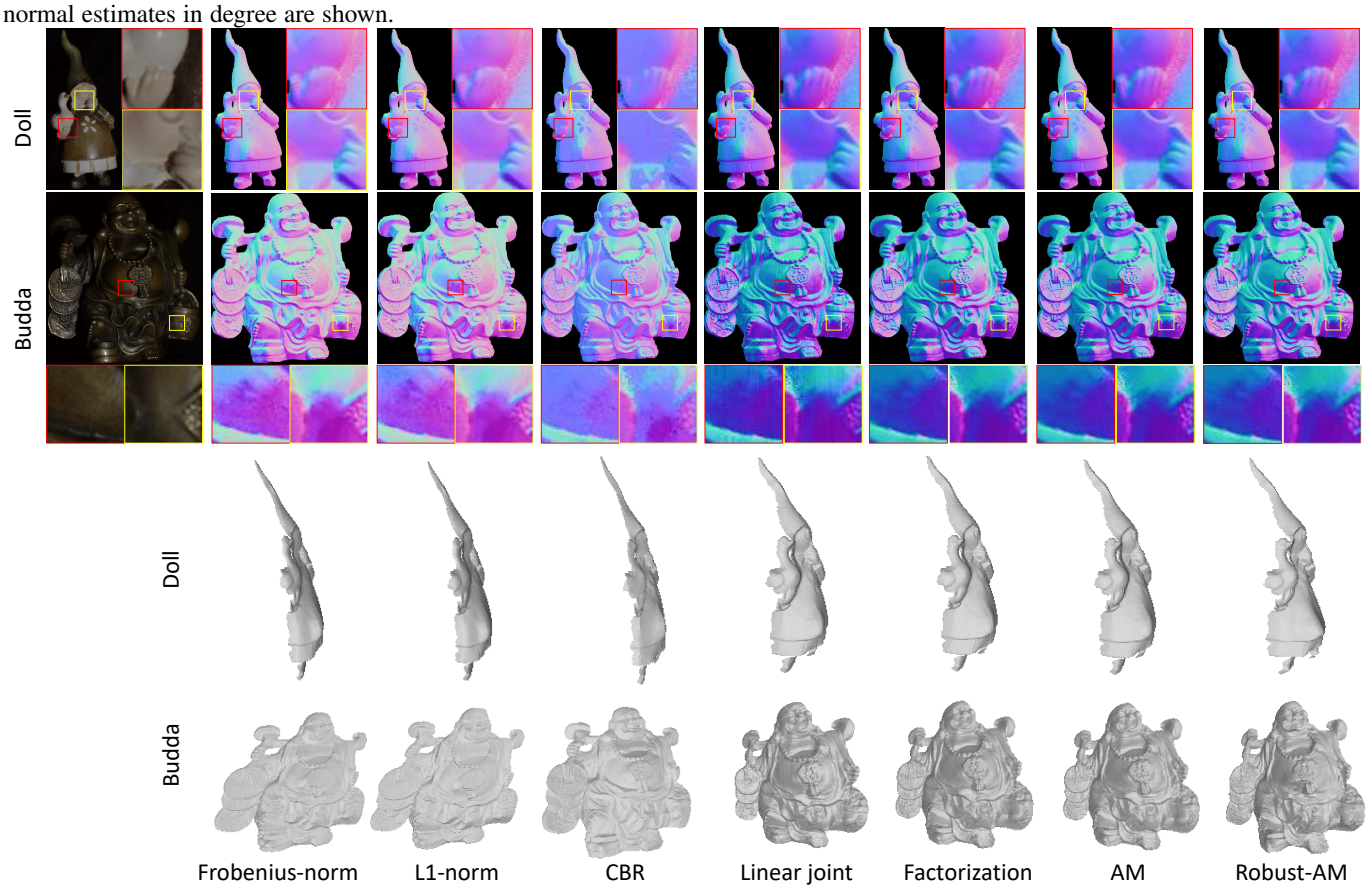

Fig. 6: Result of varying light source intensities case. From left to right, one of input images, results from Frobenius-norm, L1-norm, CBR [25], linear joint estimation, factorization, alternating minimization (AM) and Robust-AM methods are shown.

of properly handling varying light intensities and exposures.

REFERENCES

[1] R. J. Woodham, "Photometric method for determining surface orientation from multiple images," *Optical Engineering*, vol. 19, no. 1, pp. 139–144, January 1980.

[2] T. Wu, K. Tang, C. Tang, and T. Wong, "Dense photometric stereo: A markov random field approach," *IEEE Trans. Pattern Anal. Mach. Intell. (TPAMI)*, vol. 28, no. 11, pp. 1830–1846, 2006.

[3] F. Verbiest and L. Van Gool, "Photometric stereo with coherent outlier handling and confidence estimation," in *Proc. of Computer Vision and Pattern Recognition (CVPR)*, 2008.

[4] L. Wu, A. Ganesh, B. Shi, Y. Matsushita, Y. Wang, and Y. Ma, "Robust photometric stereo via low-rank matrix completion and recovery," in *Proc. of Asian Conf. on Computer Vision (ACCV)*, 2010.

[5] T.-H. Oh, H. Kim, Y.-W. Tai, J.-C. Bazin, and I. S. Kweon, "Partial sum minimization of singular values in rpca for low-level vision," in *Proc. of Int'l Conf. on Computer Vision (ICCV)*, 2013.

[6] Y. Zhang, C. Mu, H.-W. Kuo, and J. Wright, "Toward guaranteed illumination models for non-covex objects," in *Proc. of Int'l Conf. on Computer Vision (ICCV)*, 2013.

[7] D. Cho, Y. Matsushita, Y.-W. Tai, and I. S. Kweon, "Photometric stereo under non-uniform light intensitiesand exposures," in *ECCV*, 2016.

[8] H. Hayakawa, "Photometric stereo under a light-source with arbitrary motion," *Journal of the Optical Society of America (JOSA)*, vol. 11, no. 11, pp. 3078–3089, 1994.

[9] A. L. Yuille and D. Snow, "Shape and albedo from multiple images using integrability," in *Proc. of Computer Vision and Pattern Recognition (CVPR)*, 1997, pp. 158–164.

[10] P. N. Belhumeur, D. J. Kriegman, and A. L. Yuille, "The bas-relief ambiguity," *Int'l Journal of Computer Vision (IJCV)*, vol. 35, no. 1, pp. 33–44, 1999.

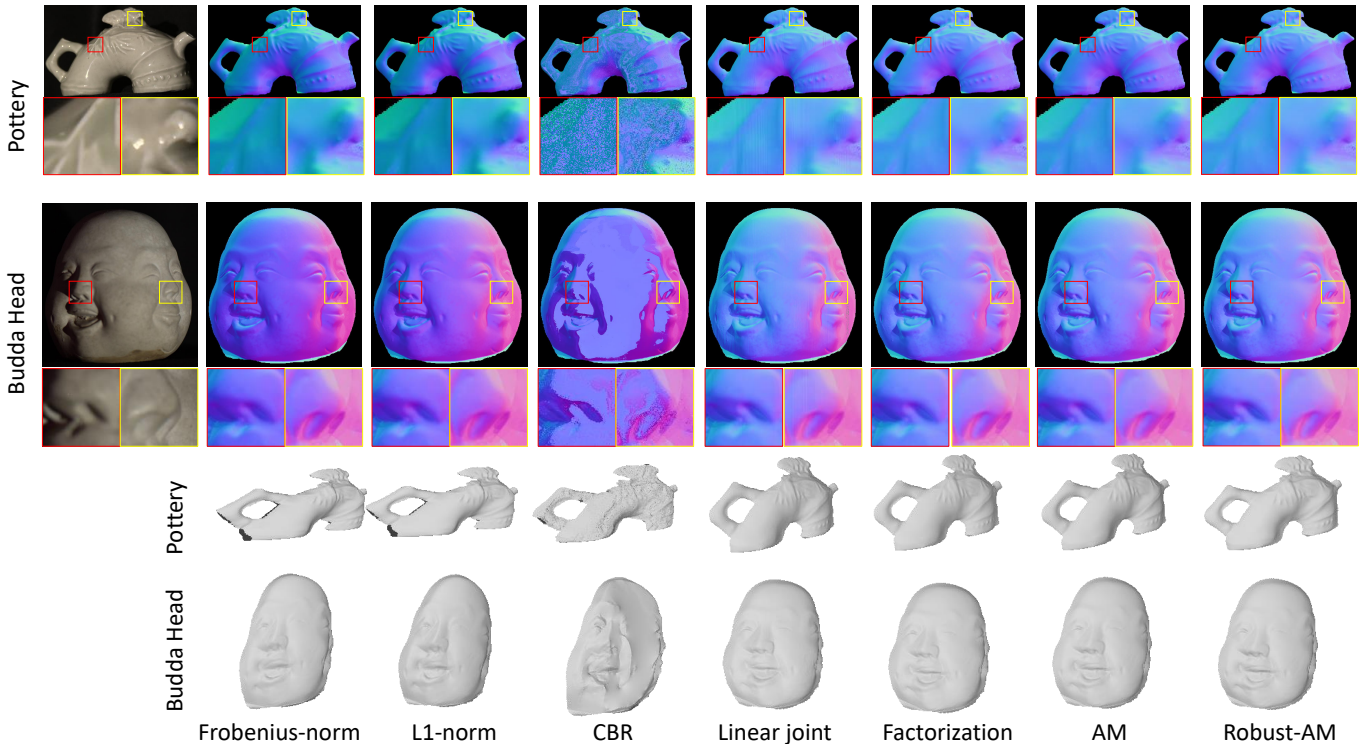

Fig. 7: Result of auto-exposure case. From left to right, one of input images, results from Frobenius-norm, L1-norm, CBR [25], linear joint estimation, factorization, alternating minimization (AM) and Robust-AM methods are shown.

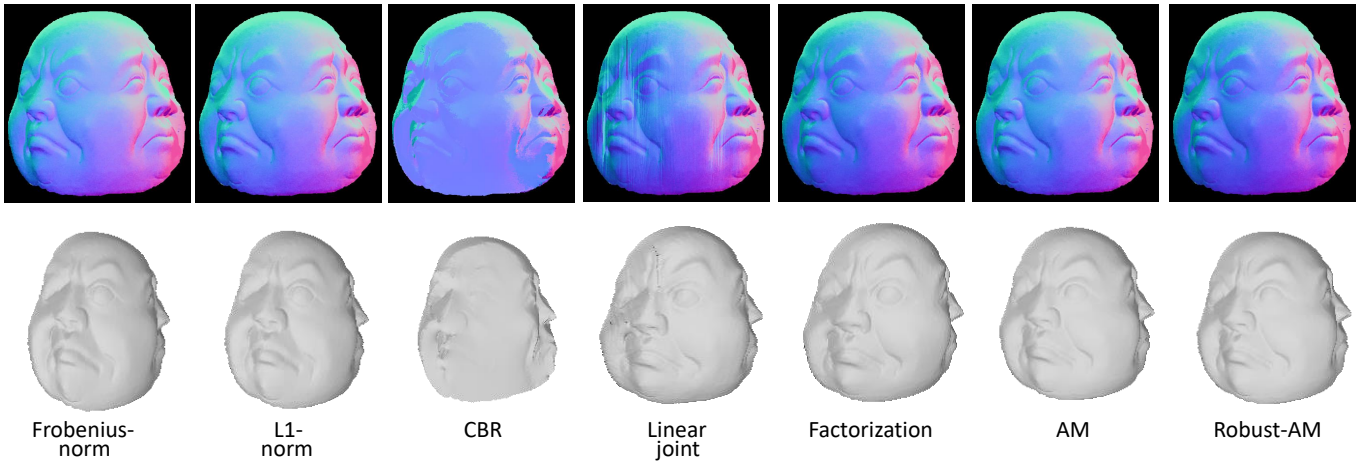

Fig. 8: Result using a mobile phone camera. Top: Estimated surface normal, Bottom: 3D reconstruction. Our methods (linear joint estimation, factorization, alternating minimization (AM) and Robust-AM methods) produce more faithful results than the conventional methods.

[11] N. G. Alldrin, S. P. Mallick, and D. J. Kriegman, "Resolving the generalized bas-relief ambiguity by entropy minimization," in *Proc. of Computer Vision and Pattern Recognition (CVPR)*, 2007.

[12] O. Drbohlav and M. Chantler, "Can two specular pixels calibrate photometric stereo?" in *Proc. of Int'l Conf. on Computer Vision (ICCV)*, 2005, pp. 1850–1857.

[13] K. Sunkavalli, T. Zickler, and H. Pfister, "Visibility subspaces: Uncalibrated photometric stereo with shadows," in *Proc. of European Conf. on Computer Vision (ECCV)*, 2010, pp. 251–264.

[14] B. Shi, Y. Matsushita, Y. Wei, C. Xu, and P. Tan, "Self-calibrating photometric stereo," in *Proc. of Computer Vision and Pattern Recognition (CVPR)*, 2010, pp. 1118–1125.

[15] F. Solomon and K. Ikeuchi, "Extracting the shape and roughness of specular lobe objects using four light photometric stereo," *IEEE Trans. Pattern Anal. Mach. Intell. (TPAMI)*, vol. 18, no. 4, pp. 449–454, 1996.

[16] A. Georghiades, "Incorporating the torrance and sparrow model of reflectance in uncalibrated photometric stereo," in *Proc. of Int'l Conf. on Computer Vision (ICCV)*, 2003, pp. 816–823.

[17] S. Lin and S. W. Lee, "Estimation of diffuse and specular appearance," in *Proc. of Int'l Conf. on Computer Vision (ICCV)*, 1999, pp. 855–860.

[18] H. T. Y. Iwahori, R. J. Woodham and N. Ishii, "Neural network to reconstruct specular surface shape from its three shading images," in *Proc. International Joint Conference on Neural Networks*, 1993, pp. 1181–1184.

[19] T. Malzbender, B. Wilburn, D. Gelb, and B. Ambrisco, "Surface enhancement using real-time photometric stereo and reflectance transformation," in *Proceedings of the Eurographics Symposium on Rendering Techniques*, 2006, pp. 245–250.

[20] B. Shi, P. Tan, Y. Matsushita, and K. Ikeuchi, "Bi-polynomial modeling of low-frequency reflectances," *IEEE Trans. Pattern Anal. Mach. Intell. (TPAMI)*, vol. 36, no. 6, pp. 1078–1091, 2014.

[21] S. Ikehata, D. P. Wipf, Y. Matsushita, and K. Aizawa, "Photometric

	Sphere		Textured		Caesar	
Condition	Spatial varying	Non-uniform	Spatial varying	Non-uniform	Spatial varying	Non-uniform
NLPS [29]	**0.002**	5.212	**0.002**	5.212	**0.184**	5.342
AM	3.469	**1.7555e-06**	3.443	**2.3556e-06**	4.066	**2.0298e-06**

TABLE 3: Comparison of methods under spatially-varying and non-uniform (ours) light settings. The NLPS method shows lower accuracy for the non-uniform intensity case, while it is effective in the spatially-varying light setting. Our method works in a complementary manner; it does not handle the spatially-varying light case, but is effective for non-uniform light and exposure case.

stereo using sparse bayesian regression for general diffuse surfaces," *IEEE Trans. Pattern Anal. Mach. Intell. (TPAMI)*, vol. 36, no. 9, pp. 1816–1831, 2014.

[22] J. Sylvester, "Sur lequations en matrices px = xq," *C. R. Acad. Sc. Paris*, vol. 99, no. 2, pp. 67–71,115–116, 1884.

[23] P. W. Holland and R. E. Welsch, "Robust regression using iteratively reweighted least-squares," *Communications in Statistics: Theory and Methods*, vol. 6, no. 9, pp. 813–827, 1977.

[24] B. Kamgar-Parsi and B. Kamgar-Parsi, "Evaluation of quantization error in computer vision," *C. R. Acad. Sc. Paris*, vol. 11, no. 9, pp. 929–940, 1989.

[25] S. Ikehata and K. Aizawa, "Photometric stereo using constrained bivariate regression for general isotropic surfaces," in *Proc. of Computer Vision and Pattern Recognition (CVPR)*, 2014.

[26] B. Shi, Z. Wu, Z. Mo, D. Duan, S.-K. Yeung, and P. Tan, "A benchmark dataset and evaluation for non-lambertian and uncalibrated photometric stereo," in *Proc. of Computer Vision and Pattern Recognition (CVPR)*, 2016.

[27] W. Xie, Y. Zhang, C. C. L. Wang, and R. C.-K. Chung, "Surface-from-gradients: An approach based on discrete geometry processing," in *Proc. of Computer Vision and Pattern Recognition (CVPR)*, 2014.

[28] J.-Y. Lee, Y. Matsushita, B. Shi, I. S. Kweon, and K. Ikeuchi, "Radiometric calibration by rank minimization," *IEEE Trans. Pattern Anal. Mach. Intell. (TPAMI)*, vol. 35, no. 1, pp. 144–156, Jan. 2013.

[29] T. Papadhimitri and P. Favaro, "Uncalibrated near-light photometric stereo," in *Proceedings of the British Machine Vision Conference*. BMVA Press, 2014.

[30] F. Sakaue and J. Sato, "A new approach of photometric stereo from linear image representation under close lighting," in *Proc. of Int'l Conf. on Computer Vision Workshops (ICCV Workshops)*, 2011, pp. 759 – 766.

[31] W. Xie, C. Dai, and C. C. L. Wang, "Photometric stereo with near point lighting: A solution by mesh deformation," in *Proc. of Computer Vision and Pattern Recognition (CVPR)*, 2015.

Donghyeon Cho is a Ph.D. student in EE department of KAIST, South Korea. From Sept 2014 to Feb 2015, he worked as a full-time student internship in the Microsoft Research Asia (MSRA). He received the MS degree in Computer Science from Korea Advanced Institute of Science and Technology (KAIST), Daejeon, Korea in 2014. He received the BS degree in information and communication engineering from Inha University, Incheon, Korea, in 2012. His research interests include image/video processing, computer vision and computational photography. He is a student member of the IEEE.

Yasuyuki Matsushita received his B.S., M.S. and Ph.D. degrees in EECS from the University of Tokyo in 1998, 2000, and 2003, respectively. From April 2003 to March 2015, he was with Visual Computing group at Microsoft Research Asia. In April 2015, he joined Osaka University as a professor. His research area includes computer vision, machine learning and optimization. He is on the editorial board of IEEE Transactions on Pattern Analysis and Machine Intel- ligence (TPAMI), International Journal of Computer Vision (IJCV), IPSJ Journal of Computer Vision and Applications (CVA), The Visual Computer Journal, and Encyclopedia of Computer Vision. He served/is serving as a Program Co-Chair of PSIVT 2010, 3DIMPVT 2011, ACCV 2012, ICCV 2017, and a General Co-Chair for ACCV 2014. He is a senior member of IEEE.

Yu-Wing Tai is a research director of youtu research lab of Tencent SNG. He was a principle research scientist of SenseTime Group Limited from September 2015 to December 2016. He was an associate professor working at the Korea Advanced Institute of Science and Technology (KAIST) from July 2009 to August 2015. He received his Ph.D. degree in Computer Science from the National University of Singapore (NUS) in 2009. From Sept 2007 to June 2008, he worked as a full-time student internship in the Microsoft Research Asia (MSRA). He was awarded the Microsoft Research Asia Fellowship in 2007, and the KAIST 40th Anniversary Academic Award for Excellent Professor in 2011 respectively. He received a M.Phil and B.Eng (First Class Honors) degree in Computer Science from the Hong Kong University of Science and Technology (HKUST) in 2005 and 2003 respectively. He is a senior member of the IEEE.

Inso Kweon is an professor in EE department of KAIST, South Korea. He received the BS and MS degrees in mechanical design and production engineering from Seoul National University, Seoul, Korea, in 1981 and 1983, respectively, and the PhD degree in robotics from the Robotics Institute, Carnegie Mellon University, Pittsburgh, Pennsylvania, in 1990. He worked for the Toshiba R&D Center, Japan, and joined the Department of Automation and Design Engineering, KAIST, Seoul, Korea, in 1992, where he is now a professor with the Department of Electrical Engineering. He is a recipient of the best student paper runner-up award at the IEEE Conference on Computer Vision and Pattern Recognition (CVPR 09). His research interests are in camera and 3D sensor fusion, color modeling and analysis, visual tracking, and visual SLAM. He was the program co-chair for the Asian Conference on Computer Vision (ACCV 07) and was the general chair for the ACCV 12. He is also on the editorial board of the International Journal of Computer Vision. He is a member of the IEEE and the KROS.